J Mater Sci: Mater Med (2011) 22:1–9
DOI 10.1007/s10856-010-4179-1

Characterization of the chemically deposited hydroxyapatite coating on a titanium substrate

Alexander V. Zavgorodniy · Oscar Borrero-López · Mark Hoffman · Racquel Z. LeGeros · Ramin Rohanizadeh

Received: 6 September 2010 / Accepted: 25 October 2010 / Published online: 5 November 2010

Abstract Bioactive hydroxyapatite (HA) coating on titanium (Ti) implant can be used as a drug delivery device. A controlled release of drug around the implant requires the incorporation of drug into the coating material during the coating process. HA coating was prepared using a two-step procedure in conditions suitable for simultaneous incorporation of the protein-based drug into the coating material. Monetite coating was deposited on Ti substrate in acidic condition followed by the transformation of the monetite coating to HA. X-ray diffraction (XRD) confirmed the formation of the monetite phase at the first step of the coating preparation, which was transformed into HA at the second step. Fourier transform infrared spectroscopy demonstrated typical bands of a crystallized carbonated HA with A- and B-type substitution, which was confirmed by the XRD refinement of the structural parameters. Scanning electron microscope was used to observe the morphology of monetite and HA coatings. Adhesion of the coatings was measured using a scratch tester. The critical shearing stress was found to be 84.20 ± 1.27 MPa for the monetite coating, and 44.40 ± 2.39 MPa for the HA coating.

A. V. Zavgorodniy (✉) · R. Rohanizadeh
Faculty of Pharmacy, University of Sydney, Pharmacy Building (A15), Science Road, 2006 New South Wales, Australia
e-mail: alexander.zavgorodniy@sydney.edu.au

O. Borrero-López
Departamento de Ingeniería Mecánica, Energética y de los Materiales, Escuela de Ingenierías Industriales, Universidad de Extremadura, Avenida de Elvas, s/n, Badajoz 06071, Spain

O. Borrero-López · M. Hoffman
Department of Materials Science and Engineering, University of New South Wales, 2052 New South Wales, Australia

R. Z. LeGeros
College of Dentistry, New York University, New York 10100, USA

1 Introduction

Symptomatic osteoarthritis of the hip or knee is the major contributor to a functional impairment and social isolation in older adults [1]. In advanced stages of osteoarthritis of hips or knees, medications and physical therapy are of a limited value [2, 3]. Joint replacement can effectively alleviate pain and restore function [4, 5].

Pure titanium is one of the metallic biomaterials widely used today in replacing hard tissue due to its excellent specific strength, corrosion resistance, no inflammatory or immunogenic reactions and superior biocompatibility among other metallic biomaterials [6, 7]. However, titanium and its alloys fall into a group of bioinert materials and their biocompatibility is inferior to that of calcium phosphates, such as hydroxyapatite (HA). Thus, a modification of the surface of a Ti implant, which will promote a higher osteointegration of such implant is essential. Such systems combine the mechanical advantage of the metallic substrate and the biological affinity of the HA surface to bone. It is critical, however, that such system does not lose the interfacial integrity during the lifetime of the orthopedic implant. Plasma spraying method [8–10] has been widely used for this purpose and received commercial success. Interfacial bonding strength for plasma sprayed HA on Ti alloys is sufficient, 20–30 MPa [11], due to development of a chemical bonding between HA and Ti through calcium titanate phase or Ti–P compounds. However, the percentage of revision operations is still very high [12]. Plasma spraying operates under extremely high temperatures, 6,000–10,000°C, and thus can easily destabilise crystal

structure of the HA, causing its decomposition into a mixture of HA, calcium oxide, tricalcium phosphate, tetracalcium phosphate and considerable amount of amorphous phases. Cracking of the coated layer is often observed, primarily due to rapid temperature fluctuations and solidification of the coating. Additionally, transformation of the amorphous phase to crystalline oxide, while the plasma-sprayed coating is subject to annealing, gives rise to cracking as a result of volume change (shrinkage). These cracks may also cause loss of adhesion of the coating, leading to coating delamination, premature wear and, finally, implant failure.

The advances in synthesis of HA coatings include RF magnetron sputter [13–15], ion-beam dynamic mixing [16–18], pulse laser deposition [19–21], sol–gel [22–24], electrochemical deposition [14, 25, 26] and recently, chemical deposition [27–29]. The chemical deposition method receives high attention not only because of its ease processing and forming but most importantly because of its low temperature nature, below 100°C, which may allow the incorporation, and therefore controlled release, of an osteoinductive drug, such as bone morphogenetic proteins into the coating during the HA coating deposition process. Such a drug delivery system may reduce the healing time after the operation and the risk of a revision surgery.

In this work we investigate the chemical deposition of a monetite coating, followed by the hydrothermal conversion of the monetite coating into HA coating in alkali solution at the temperature below 100°C. This method could be useful for potential protein-based drug incorporation into the coating materials, such as BMP-2, at the monetite-to-apatite conversion stage of the coating preparation. The incorporation of the drug during the process of the coating formation will ensure a sustained release of the drug into the surrounding tissue after the joint replacement surgery. The other important advantage of this method in comparison with the plasma spraying is the possibility to deposit an homogenous HA coating on dental and orthopedic implants with complex geometry (internal cavity) or macroporosities. This coating method is simple and low cost—advantages for use in the biomaterials industry. Therefore the goal of this work was to prepare and characterize a homogenous HA coating on Ti substrate suitable for hip and knee replacement applications in the conditions, which allow the simultaneous incorporation of the protein-based drugs, such as BMP-2, into the HA coating material.

2 Materials and methods

2.1 Coating preparation

HA coating on Ti discs (15 mm in diameter and 1 mm thick) was prepared using chemical deposition method. The coating solution was prepared using calcium carbonate, $CaCO_3$ (MP Biomedicals, USA) and sodium phosphate dibasic anhydrous, NaH_2PO_4 (MP Biomedicals, USA) as raw materials. These reagents were mixed in deionized ultrapure water (mol. ratio $CaCO_3$: NaH_2PO_4 = 1:1, concentration 0.2 M). Phosphoric acid was added until the reagents were completely dissolved and the final pH was 2.77. Ti coupons were polished to 600 grit and then ultrasonically cleaned in the following sequence of baths: deionized ultrapure water, acetone, deionized ultrapure water, ethanol, deionized ultrapure water (10 min in each bath). Air-dried Ti coupons were immersed into the coating solution for 24 h at 75°C. Coated Ti coupons were rinsed in deionized ultrapure water, air dried and then immersed into 0.2 M sodium hydroxide solution for 24 h at 75°C for the hydrothermal treatment. Ti coupons were then rinsed in deionized ultrapure water and air dried.

2.2 Coating characterization

The phase composition of the coating was analysed using X-ray diffraction (XRD, S6000, Schimadzu, Japan) with a step size of 0.02° at a scanning rate of 1° min^{-1}. The structural analysis of X-ray diffraction patterns was undertaken using the Le Bail [30] method as implemented in the Rietica software package [31]. Infrared (IR) spectra were measured using Fourier transform infrared (FTIR) spectrometer (FT-IR Varian 610-IR, Varian Inc., USA) with the resolution 4 cm^{-1}. The accuracy of measurements was ± 0.5 cm^{-1} and the number of scans was 32. Surface morphology and the composition of the coated Ti coupons were analyzed using scanning electron microscope (SEM, Ultra plus, Zeiss, Germany) coupled with energy-dispersive spectrometer (EDS, Zeiss, Germany). The profile and the roughness of the coatings were measured using atomic force microscope (AFM, Nanoscope IIIa controller, Veeco Inc., USA) with a tapping mode.

For evaluation of the coating thickness, three Ti discs coated with monetite and three Ti discs coated with HA were fixed in poly-methylmethacrylate (PMMA) and two sections from each disc were cut using a diamond saw (Isomet Low Speed, Buehler, Germany). The sections were subsequently grounded and polished with a micro grinding system (Allied High Tech, USA) before the analyses under SEM.

Scratch tests were used to estimate the adhesion strength of the coatings to the Ti substrate according to procedures outlined in ASTM C1624–05 [32]. Normal load applied to a diamond tip (Rockwell C, 200 μm radius) was increased from 1 to 6 N, a loading rate of 10 N/min and sliding speed of 10 mm/min over a 5 mm scratch line to find the critical strength for coating failure. SEM was used to identify mechanical events occurred along the scratch lines and the

critical load was defined at the onset of coating detachment from the substrate. Altogether, four Ti discs coated with monetite and four Ti discs coated with HA were tested; five scratch tests were performed on each disc. Hardness and elastic modulus of the Ti substrate and the coating were measured according to the Oliver and Pharr method [33], using a UMIS-2000 ultra-micro indentation system equipped with a Berkovich indenter. For the evaluation of hardness and elastic modulus of the Ti substrate, ten measurements were performed at maximum load of 50 mN and, for the evaluation of hardness and elastic modulus of the HA coatings, ten measurements were performed at a maximum load of 1 mN in order to maintain the indentation depth below 10% of the coating thickness.

3 Results

Chemical analysis of the coatings deposited on a Ti surface using chemical deposition method confirmed that the coatings consisted of calcium phosphates (Fig. 1a). The structural analysis of the coatings revealed that the measured XRD profiles (Fig. 1b) are in good agreement with the reference data JCPDS 70-0360 ($CaHPO_4$, monetite).

SEM observations of the morphology of the deposited coatings revealed that the thickness of the coating was 20 μm. The coating consisted of smooth, plate-like monetite crystals (Fig. 1c and d), which agglomerated together and formed a dense structure. Monetite crystals had dimensions of 20 × 10 × 5 μm.

After the 24 h hydrothermal treatment in sodium hydroxide alkaline solution of the Ti discs, coated with monetite crystals, the chemical composition of the coatings was examined using the EDS. The coating consisted of Ca, P, O elements (Fig. 2a), the traces of Na and Si were also detected.

The structural analysis of the coating (Fig. 2b) demonstrated that only HA characteristic peaks were present in the XRD pattern, which were indexed according to the reference data JCPDS 09-0432. The peaks broadening in the XRD patterns could be attributed to the relatively small, nanometer size of the HA crystals, which was confirmed by the SEM observations (Fig. 3a). The results of the refinement analysis of the HA coating are presented in Fig. 2b and Table 1.

The FTIR analysis of the coating (Fig. 2c) revealed bands, which are characteristic to HA. The IR spectrum was dominated by the PO_4 bands typical to the apatite phase, i.e. triply degenerated ν_3PO_4 asymmetric mode at 1,086 (shoulder) and 1,018 cm^{-1}, non-degenerated symmetric stretching mode of ν_1PO_4 at 962 cm^{-1} and the components of the triplet of ν_4PO_4 bending mode at 625 cm^{-1} and 600 cm^{-1}. Overlapping carbonate bands were observed at 1,550–1,350 cm^{-1} (ν_3), 875 cm^{-1} (ν_2) and 710 cm^{-1} (ν_4). The broad band of low intensity in the high energy region (3,600–3,000 cm^{-1}) together with the weak band around 1,640 cm^{-1} of the

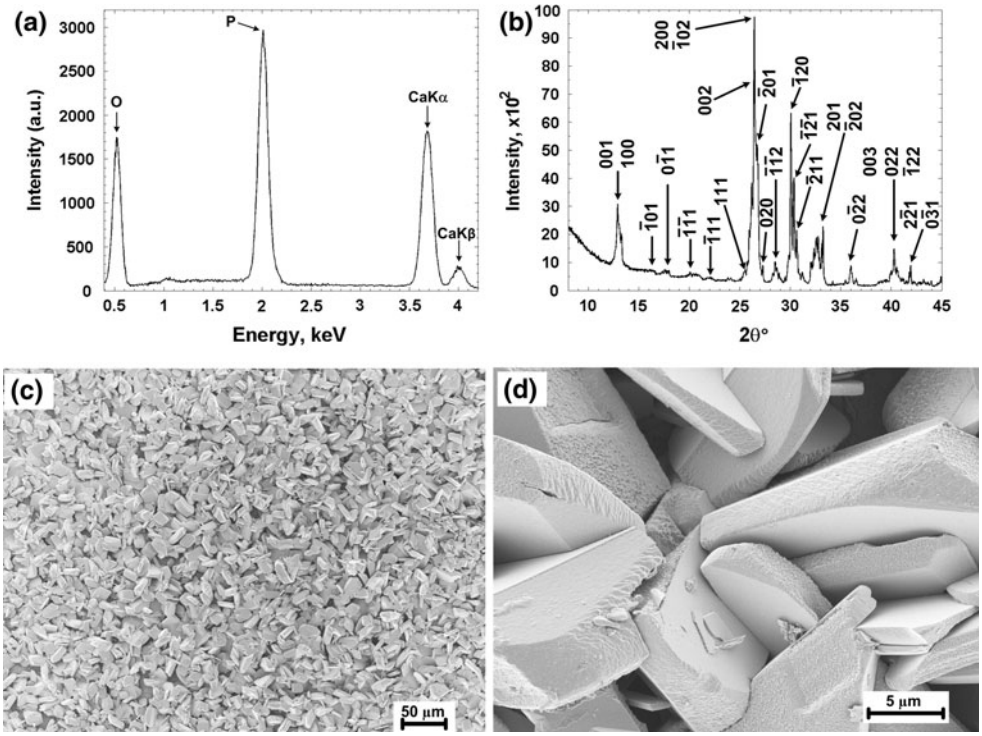

Fig. 1 EDS analysis of chemical composition of the monetite coating (**a**) and the XRD profile of the coating (**b**). SEM morphology of the monetite coating crystals (**c**, **d**)

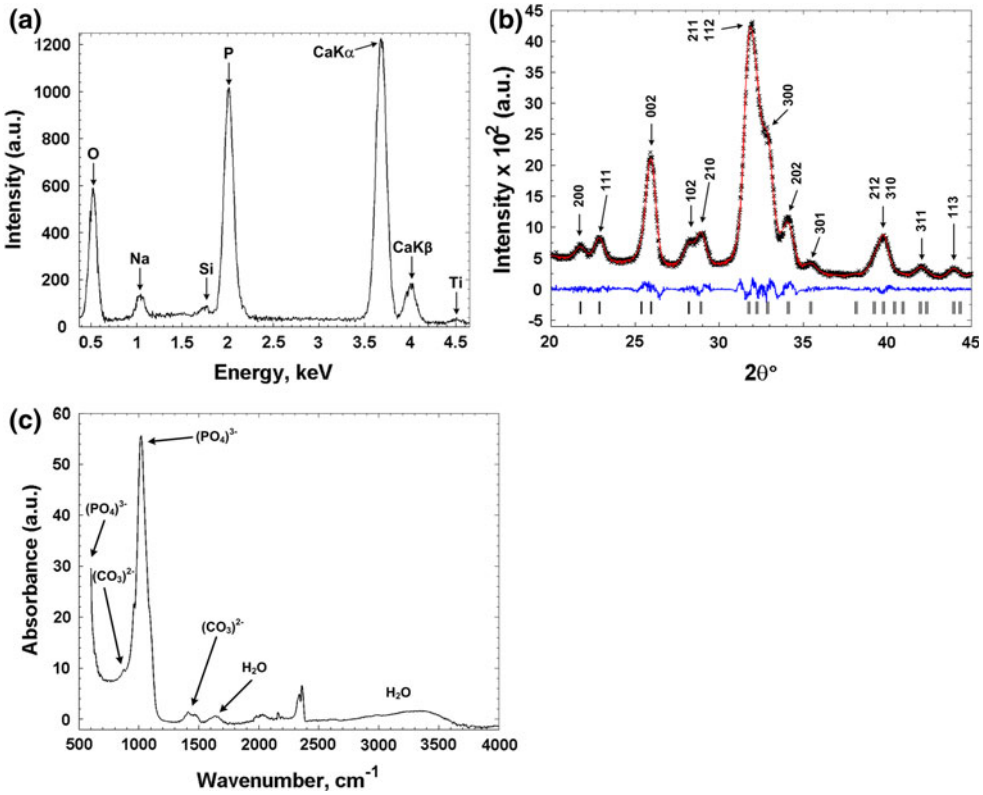

Fig. 2 **a** EDS analysis of chemical composition of the HA coating. **b** XRD profile of the coating. The calculated plot is presented as a continuous line through the data points. The residues plot and the position of the peaks of the HA phase are presented below the XRD profile. **c** FTIR spectrum of the HA coating

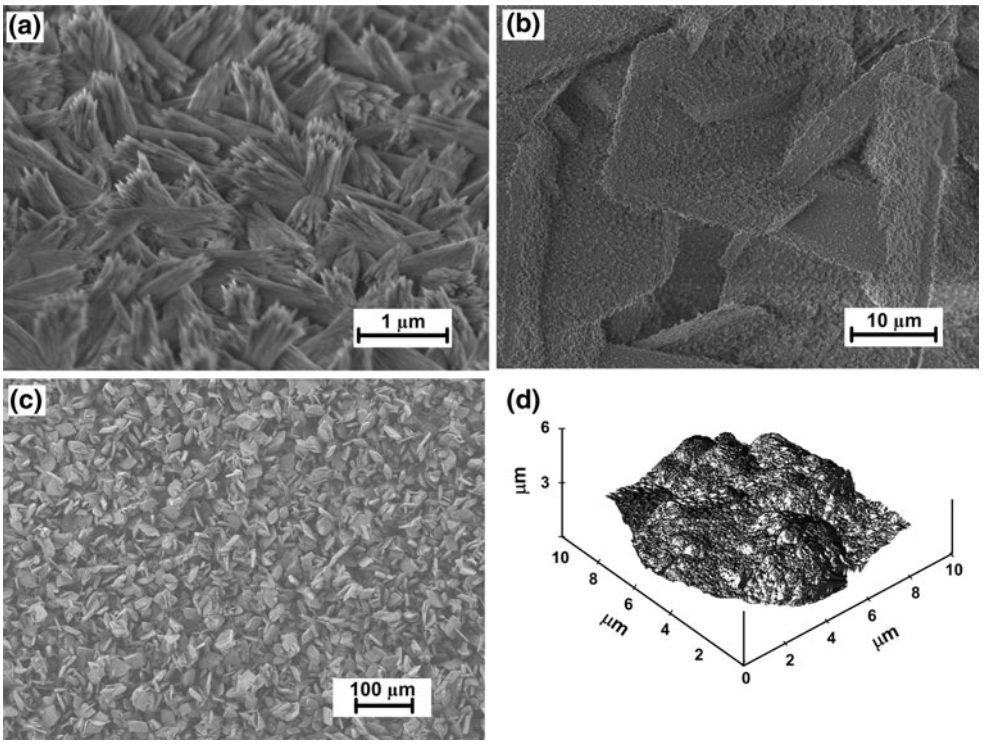

Fig. 3 SEM image of the HA coating morphology (**a**, **b** and **c**) and the AFM topographical image of the HA coating (**c**)

H–O–H bending mode was assigned to the traces of water incorporated into the crystal lattice of the structure [34, 35]. The band, which corresponds to the stretching vibration of the OH^- group at 3,570 cm^{-1} was observed.

The SEM observations of the HA coating revealed that the thickness of the coating remained 20 µm and it consisted of nano-sized bundles of needle-like HA crystals (Fig. 3a), which were agglomerated together following the

Table 1 Refined structural parameters of the coating. Space group $P6_3/m$ (hexagonal), $\alpha = \beta = 90°$, $\gamma = 120°$. Cell parameters (a, c), profile residues (Rp) and weighted profile residues (Rwp) are presented

a (Å)	*c* (Å)	R_p (%)	R_{wp} (%)
9.436(3)	6.867(2)	3.53	4.75

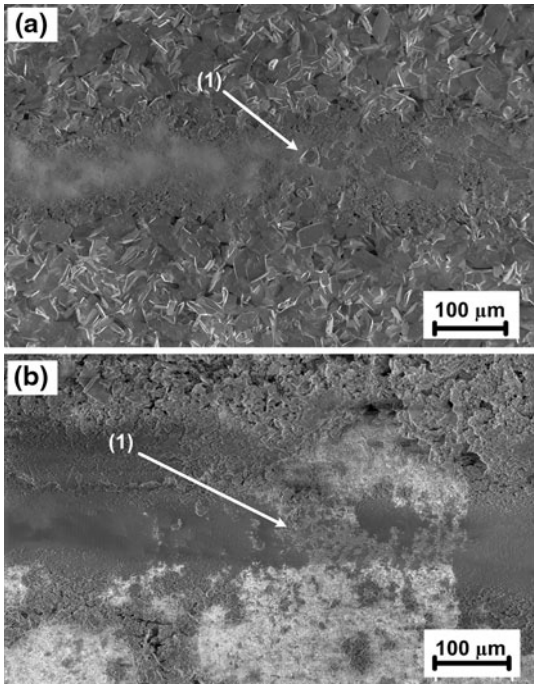

Fig. 4 **a** SEM image of the end of the scratch line (*arrow 1*) through the monetite coating. *Arrow (1)* shows the first failure of the coating. **b** SEM image of the scratch line through the HA coating. *Arrow (1)* shows the buckling failure of the coating

geometry of the large plate-like shape of the precursor monetite crystals (Fig. 3b and c). Profile (Fig. 3d) and the average roughness of the HA coating, Ra = 362 nm, was measured using AFM.

The scratch experiments showed that the monetite coating starts to deform plastically at the initial load of 1 N followed a continuous smooth-based scratch formation (Fig. 4a). Monetite coatings typically exhibited their first catastrophic failure (i.e. exposure of the substrate; Fig. 4a, *arrow 1*) at normal loads of 5.2–5.6 N with a corresponding friction force of approximately 1.4 N. The critical normal force was determined from the analysis of the scratch tracks in the SEM to locate the position of a failure. The corresponding normal and tangential forces were then identified from the curves measured by the scratch tester.

Scratch experiments on the HA coatings showed the first catastrophic failure typically at normal loads 1.3–1.7 N (Fig. 4b, *arrow 1*), corresponding to a friction force of approximately 0.5 N.

4 Discussion

4.1 Deposition of monetite

In the presented study HA coating was prepared on a Ti substrate in mild conditions using chemical deposition method, which may allow the incorporation of a protein based drug into the coating. HA coating was prepared in two stages. At the first stage a calcium phosphate coating was produced in the acidic conditions at pH = 2.77. The calcium phosphate nature of the coating was confirmed by EDS (Fig. 1a). According to the solubility diagrams of calcium phosphates [36], monetite is the most stable phase of calcium phosphates in acidic conditions with pH < 5. The XRD analysis of the coating confirmed, that the only phase of the coating was monetite (Fig. 2a). Stoichiometric molar calcium phosphate ratio of monetite is 1, while EDS analysis revealed that the calcium phosphate ratio of the coating was approximately 0.84. This result suggests a defective structure of the monetite crystals with a high concentration of Ca vacancies in the lattice structure.

The pH of the solution was 2.77, which was below the point of zero charge (PZC) of TiO_2, pH 5.9 [37], therefore the surface of the Ti was positively charged (Fig. 5) [38]:

$$Ti^{IV} - O + H^+ \rightarrow Ti^{IV} - O - H^+ \quad (1)$$

Using X-ray photoelectron spectroscopy (XPS), it has been demonstrated that this positively charged layer attracts negatively charged PO_4^{3-} ionic species from the

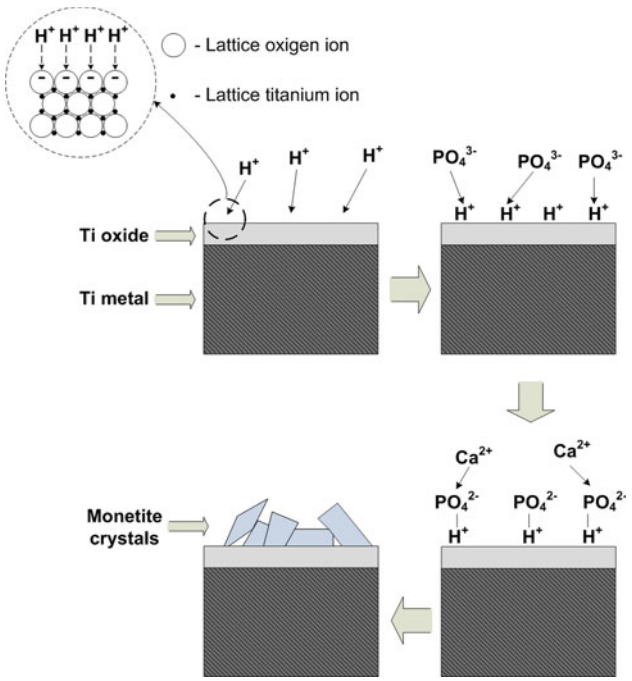

Fig. 5 Schematic representation of the surface reaction of the monetite formation on the Ti substrate

bulk of the electrolyte solution (Fig. 5), followed by the Ca^{2+} ionic species to compensate the formation of the negative charge [39]. In this region, there is an excess of the ion concentration of the opposite charge in respect to the equilibrium concentration, which in turn results in the greater long range Coulomb interactions between the pairs of ions, giving raise of the structural order in the neighborhood of the ions and, consequently, the nucleation and growth of crystals. The Debye-Hückel approximation of the mean-field Poisson-Boltzmann equation introduces the Debye length parameter [40], which indicates the distance from the charged surface of the substrate into the bulk of the electrolyte solution, where the electrical charge and the thermal energy are balanced (Fig. 6a):

$$\lambda_D^2 = \frac{\varepsilon\varepsilon_0 k_B T}{\sum_k n_k q_k} \tag{2}$$

Here, ε is the dielectric permittivity of the solvent, ε_0 is the permittivity of vacuum, k_B is the Boltzmann's constant, T is the absolute temperature, n_k is the number density of ion species k, q_k is the charge of the ion of species k. Substitution of the ionic strength of the electrolyte solution $I = \frac{1}{2}\sum_k c_k z_k$, where c_k is the molar concentration of the ion species k and z_k is the valence of the ion species k, into the Eq. 2, gives:

$$\lambda_D^2 = \frac{\varepsilon\varepsilon_0 k_B T}{2N_A e^2 I} \tag{3}$$

Where N_A is the Avogadro number and e is the elementary charge (Fig. 6b).

From the Eq. 3 it follows that the Debye length is much less dependent on the temperature of the system (Fig. 6b) than on the ionic strength (Fig. 6b and c). Hence, to match the values of the monetite lattice parameters ($a = 6.910$ Å, $b = 6.627$ Å, and $c = 6.998$ Å [JCPDS 70-0360]) with λ_D and in the same time to ensure the stability of protein based drugs in drug delivery applications, the temperature of the system was fixed at 75C° and the ionic strength of the solution was carefully selected at 0.2 M (Fig. 6c).

4.2 Monetite-to-apatite conversion

At the pH values above 9, the most stable calcium phosphate phase in aqueous solutions is HA [41]. At such pH values, monetite phase is unstable and monetite crystals are dissolved, making the solution at the vicinity of the monetite crystals supersaturated in respect with Ca^{2+} and PO_4^{3-} ions, followed by the precipitation of a stable HA phase at the precursor surface of monetite crystals. The transformation of monetite to HA in alkali solution has been previously described in terms of dissolution and

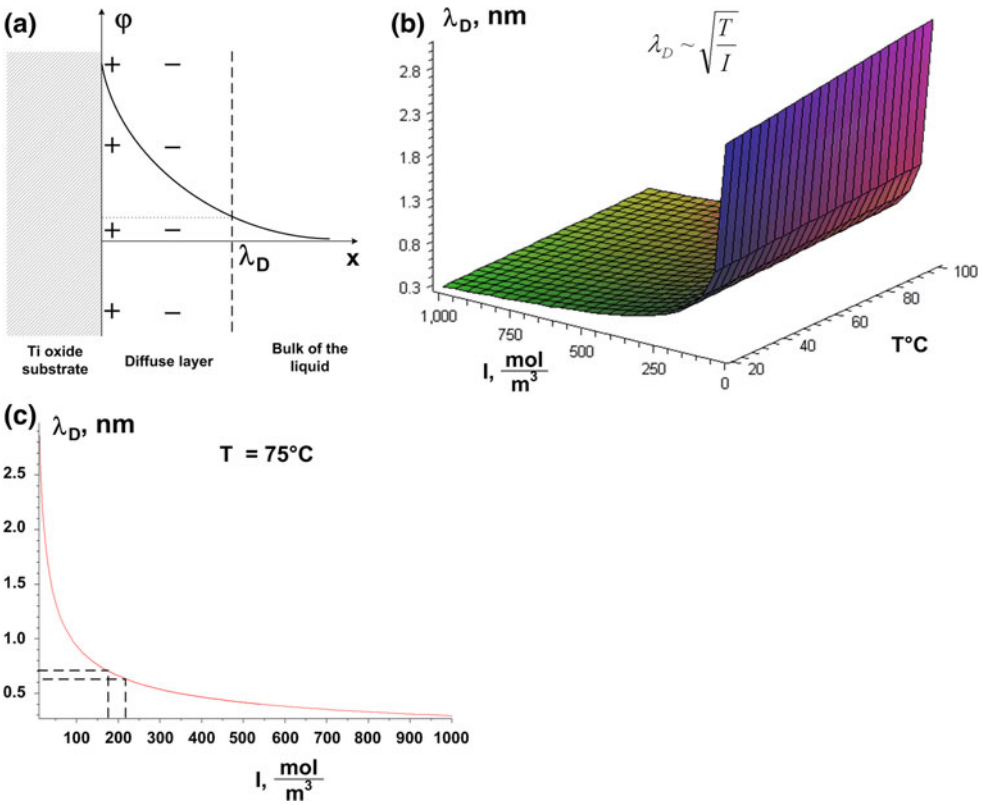

Fig. 6 **a** Schematic representation of the Ti—Electrolyte interface. **b** Dependency of the Debye length from the ionic strength of the electrolyte and temperature. **c** Dependency of the Debye length of the ionic strength at 75°C

re-precipitation processes and the proposed mechanism was described using the following equations [42]:

$$CaHPO_4 \rightarrow Ca^{2+} + HPO_4^{2-} \quad (4)$$

$$(10 - x)Ca^{2+} + 6CaHPO_4^{2-} + 2OH^- \rightarrow Ca_{10-x}(PO_4)_6(OH)_2,\ 0 < x < 1 \quad (5)$$

Taking into account results of the EDS analysis (Fig. 2a), Ca/P ratio of the deposited HA coatings was estimated and was found to be approximately 1.20. This Ca/P ratio is much lower than the molar Ca/P ratio of the stoichiometric HA, which is 1.67. Also EDS detected an appreciable quantity of sodium (Fig. 2a). This result suggests that the deposited coating is calcium deficient defect structure with high density of vacancies and with Na^+ ions partially replacing calcium. Traces of silicon were also detected by EDS (Fig. 2a). These traces of silicon was probably due to the leaching of ions of silicate from the glass walls of the beaker in a highly alkali conditions, pH = 12.84, during the conversion of monetite to HA. These EDS results suggest a possible substitution of phosphate ions by silicate $(SiO_4)^{4-}$ ions, which also yield the loss of OH^- ions [43, 44].

The FTIR results showed the position of carbonate bands at 1,550, 1,450 and around 1,412 cm^{-1}, indicating the formation of a carbonated apatite with B-type substitution, while the peaks at 1,574 and 879 cm^{-1} were assigned to the v_{3b} modes of the A-type CO_3^{2-} ions (Fig. 2c). These findings suggested that the prepared apatite coating is calcium deficient with CO_3^{2-} ions substituting both OH^- and PO_4^{3-} sites. These observations were in the agreement with the AB carbonate substitution mechanism proposed by Barralet et al. [45]. The refinement of the XRD data (Table 1) revealed an increase in a axis in comparison with the stoichiometric HA ($a = 9.418$ Å, $c = 6.884$, JCPDS 09-0432) and the contraction of the c axis, which confirmed that the substitution ions are indeed incorporated into the HA crystal lattice structure.

Taking into the account the EDS, XRD and FTIR results the general formula of the prepared HA coating can be written as follows:

$$Ca_{10-\frac{\alpha}{2}-\frac{\beta}{2}}Na_\alpha(PO_4)_{6-\beta-\gamma}(CO_3)_\beta(SiO_4)_\gamma(OH)_{2-\gamma-2\delta}(CO_3)_\delta \quad (6)$$

The nanometer size of the HA crystals, which was observed in the SEM (Fig. 3a), is comparable with the size of HA crystals, which form the mineral phase of human bone. Such compatibility may be beneficial in terms of the formation of tight implant-to-bone interface due to partial resorbtion of the upper layers of the coating by osteoclasts, followed by the formation of bone by osteoblasts.

4.3 Coating mechanical properties

SEM observations of the scratch tracks of the monetite coatings (Fig. 4) revealed that, as the load was increased in the scratch test, the monetite coating was progressively plastically deformed, thus increasing the strain at the interface, until the critical load was reached causing delamination with the substrate. Such failure mode is typical to soft coatings on harder substrates [46]. In this case, the equation of Benjamin and Weaver [47] can be used to calculate the critical shearing stress for coating removal:

$$\tau_c = \frac{kAH}{\sqrt{R^2 - A^2}} \quad (7)$$

where $A = \sqrt{\frac{L_c}{\pi H}}$ is the radius of contact, L_c is the critical load, $H = 4.04$ GPa is hardness of the substrate material, R is the radius of the diamond tip and $k = 0.2$ [48]. The failure stress induced by the indenter was calculated for monetite and the HA coatings, and the results are given in Table 2.

In general, the adhesive strength of coatings is the result of chemical bonding and mechanical interlocking between the coating and the underlying substrate. There is no direct evidence supporting the chemical bonding contribution to adhesion in HA/Ti interface in the presented system. However, the interlocking component of adhesion can be improved through surface roughening, similarly as it is done for plasma spraying. Further improvements of the interfacial bonding between ceramic coating and metallic substrate may be achieved by preparing porous titania layers using anodic oxidation of the Ti surface or oxidation of the Ti surface in hydrogen peroxide solution [27]. These layers are mainly consisted of the rutile phase and it was reported that due to the close match between the O–O distance in the (110) plane of rutile and the Ca–Ca distance in the (100) plane of the carbonate incorporated apatite, this method was found to be effective in depositing of highly adhesive apatite coatings [49]. Another promising pre-treatment method was the acid treatment of the Ti surface, followed by heat treatment. It was reported that using this method the positive charge of the Ti oxide substrate was increased and induced the formation of HA coating in the simulated body fluid (SBF) [39]. Alternative method, which achieved a high bonding strength between

Table 2 Critical load measured during scratch tests and the calculated mean failure stress

Coating	Critical load P_c, N	Failure stress, MPa
Monetite	5.45 ± 0.16	84.20 ± 1.27
HA	1.53 ± 0.16	44.40 ± 2.39

HA and Ti substrate, was the alkali treatment of the Ti substrate, followed by the heat treatment [50].

5 Conclusions

Well-crystallized and dense HA coatings were prepared on a flat Ti substrate using the two-stage process. Firstly, monetite coating was deposited using the chemical deposition technique, which was followed by the transformation of the monetite coating to the HA coating using hydrothermal process at a moderately low temperature (75°C). The prepared HA coatings were carbon-rich calcium-deficient apatite. The critical shearing stress of the HA coating was 44.40 ± 2.39 MPa, which can be used as a measure of adhesion strength of the coating under scratch. The conditions of the coatings preparation may allow the incorporation of the bone morphogenic proteins into coating materials.

Acknowledgments This study was supported by ARC Discovery Grant DP0986230. The assistance from the Electron Microscope Unit, The University of Sydney is gratefully acknowledged.

References

1. Dawson J, Linsell L, Zondervan K, Rose P, Randall T, Carr A, et al. Epidemiology of hip and knee pain and its impact on overall health status in older adults. Rheumatology. 2004;43:497–504.
2. Zhang W, Moskowitz RW, Nuki G, Abramson S, Altman RD, Arden N, et al. OARSI recommendations for the management of hip and knee osteoarthritis, Part I: critical appraisal of existing treatment guidelines and systematic review of current research evidence. Osteoarthr Cartil. 2007;15:981–1000.
3. Zhang W, Moskowitz RW, Nuki G, Abramson S, Altman RD, Arden N, et al. OARSI recommendations for the management of hip and knee osteoarthritis, Part II: OARSI evidence-based, expert consensus guidelines. Osteoarthr Cartil. 2008;16:137–62.
4. Harris WH, Sledge CB. Total hip and total knee replacement (1). N Engl J Med. 1990;323:725–31.
5. Harris WH, Sledge CB. Total hip and total knee replacement (2). N Engl J Med. 1990;323:801–7.
6. Niinomi M. Recent research and development in titanium alloys for biomedical applications and healthcare goods. Sci Technol Adv Mater. 2003;4:445–54.
7. Geetha M, Singh AK, Asokamani R, Gogia AK. Ti based biomaterials, the ultimate choice for orthopaedic implants—A review. Prog Mater Sci. 2009;54:397–425.
8. Inagaki M, Kameyama T. Phase transformation of plasma-sprayed hydroxyapatite coating with preferred crystalline orientation. Biomaterials. 2007;28:2923–31.
9. Yang S, Man HC, Xing W, Zheng X. Adhesion strength of plasma-sprayed hydroxyapatite coatings on laser gas-nitrided pure titanium. Surf Coat Technol. 2009;203:3116–22.
10. Mohammadi Z, Ziaei-Moayyed AA, Mesgar AS-M. Adhesive and cohesive properties by indentation method of plasma-sprayed hydroxyapatite coatings. Appl Surf Sci. 2007;253:4960–5.
11. Ramaswamy Y, Wu C, Zreiqat H. Orthopedic coating materials: considerations and applications. Expert Rev Med Devices. 2009;6:423–30.
12. Kurtz SM, Lau E, Ong K, Zhao K, Kelly M, Bozic KJ. Future young patient demand for primary and revision joint replacement: national projections from 2010 to 2030. Clin Orthop Relat Res. 2009;467:2606–12.
13. Wan T, Aoki H, Hikawa J, Lee JH. RF-magnetron sputtering technique for producing hydroxyapatite coating film on various substrates. Biomed Mater Eng. 2007;17:291–7.
14. Chen F, Lam WM, Lin CJ, Qiu GX, Wu ZH, Luk KDK, et al. Biocompatibility of electrophoretical deposition of nanostructured hydroxyapatite coating on roughen titanium surface: in vitro evaluation using mesenchymal stem cells. J Biomed Mater Res B Appl Biomater. 2007;82B:183–91.
15. Yan Y, Wolke JGC, De Ruijter A, Yubao L, Jansen JA. Growth behavior of rat bone marrow cells on RF magnetron sputtered hydroxyapatite and dicalcium pyrophosphate coatings. J Biomed Mater Res A. 2006;78A:42–9.
16. Ohtsuka Y, Matsuura M, Chida N, Yoshinari M, Sumii T, Dérand T. Formation of hydroxyapatite coating on pure titanium substrates by ion beam dynamic mixing. Surf Coat Technol. 1994;65:224–30.
17. Yoshinari M, Ohtsuka Y, Dérand T. Thin hydroxyapatite coating produced by the ion beam dynamic mixing method. Biomaterials. 1994;15:529–35.
18. Baszkiewicz J, Krupa D, Kozubowski JA, Rajchel B, Mitura M, Barcz A, et al. Influence of the Ca- and P-enriched oxide layers produced on titanium and the Ti6Al4 V alloy by the IBAD method upon the corrosion resistance of these materials. Vacuum. 2003;70:163–7.
19. Suda Y, Kawasaki H, Ohshima T, Nakashima S, Kawazoe S, Toma T. Hydroxyapatite coatings on titanium dioxide thin films prepared by pulsed laser deposition method. Thin Solid Films. 2006;506–507:115–9.
20. Koch CF, Johnson S, Kumar D, Jelinek M, Chrisey DB, Doraiswamy A, et al. Pulsed laser deposition of hydroxyapatite thin films. Mater Sci Eng, C. 2007;27:484–94.
21. Blind O, Klein LH, Dailey B, Jordan L. Characterization of hydroxyapatite films obtained by pulsed-laser deposition on Ti and Ti-6AL-4v substrates. Dent Mater. 2005;21:1017–24.
22. Xu W, Hu W, Li MS, Wen C. Sol-gel derived hydroxyapatite/titania biocoatings on titanium substrate. Mater Lett. 2006;60:1575–8.
23. Kim H-W, Koh Y-H, Li L-H, Lee S, Kim H-E. Hydroxyapatite coating on titanium substrate with titania buffer layer processed by sol–gel method. Biomaterials. 2004;25:2533–8.
24. Ün S, Durucan C. Preparation of hydroxyapatite-titania hybrid coatings on titanium alloy. J Biomed Mater Res B Appl Biomater. 2009;90B:574–83.
25. Kim D-Y, Kim M, Kim H-E, Koh Y-H, Kim H-W, Jang J-H. Formation of hydroxyapatite within porous TiO2 layer by micro-arc oxidation coupled with electrophoretic deposition. Acta Biomater. 2009;5:2196–205.
26. Djošić MS, Mišković-Stanković VB, Kačarević-Popović ZM, Jokić BM, Bibić N, Mitrić M, et al. Electrochemical synthesis of nanosized monetite powder and its electrophoretic deposition on titanium. Colloids Surf A. 2009;341:110–7.
27. Rohanizadeh R, Al-Sadeq M, LeGeros RZ. Preparation of different forms of titanium oxide on titanium surface: effects on apatite deposition. J Biomed Mater Res A. 2004;71A:343–52.
28. Rohanizadeh R, LeGeros RZ, Harsono M, Bendavid A. Adherent apatite coating on titanium substrate using chemical deposition. J Biomed Mater Res A. 2005;72A:428–38.

29. Rohanizadeh R, LeGeros RZ. Novel method of hydroxyapatite coating on titanium using chemical deposition. Switzerland: Key Engineering Materials: Trans Tech Publications; 2008.
30. Le Bail A. Whole powder pattern decomposition methods and applications: a retrospection. Powder Diffr. 2005;20:316–26.
31. Hunter BA, Hill RJ, Howard CJ. Rietica—a computer program for Rietveld analysis of fixed-wavelength X-ray and neutron powder diffraction patterns. NSW, Australia: Australian Atomic Energy Commission; 1995.
32. ASTM International. ASTM C1624-05. Standard test method for adhesion strength and mechanical failure modes of ceramic coatings by quantitative single point scratch testing. ASTM International, West Conshohocken, PA, USA. doi:10.1520/C1624-05
33. Oliver WC, Pharr GM. An improved technique for determining hardness and elastic modulus using load and displacement sensing indentation experiments. J Mater Res. 1992;7:1564–83.
34. Wilson RM, Elliott JC, Dowker SEP, Rodriguez-Lorenzo LM. Rietveld refinements and spectroscopic studies of the structure of Ca-deficient apatite. Biomaterials. 2005;26:1317–27.
35. Teixeira S, Rodriguez MA, Pena P, De Aza AH, De Aza S, Ferraz MP, et al. Physical characterization of hydroxyapatite porous scaffolds for tissue engineering. Mater Sci Eng, C. 2009;29:1510–4.
36. Brown PW. Phase relationships in the ternary system $CaO–P_2O_5–H_2O$ at 25°C. J Am Ceram Soc. 1992;75:17–22.
37. Schmidt J, Vogelsberger W. Aqueous long-term solubility of titania nanoparticles and titanium(IV) hydrolysis in a sodium chloride system studied by adsorptive stripping voltammetry. J Solution Chem. 2009;38:1267–82.
38. Dutta PK, Ray AK, Sharma VK, Millero FJ. Adsorption of arsenate and arsenite on titanium dioxide suspensions. J Colloid Interface Sci. 2004;278:270–5.
39. Kokubo T, Pattanayak DK, Matsushita T, Takadama H, Nakamura T. Positively charged bioactive titanium oxide formed on Ti metal by acid and heat treatments. *Bioceramics* 22: The 22nd International Simposium on Ceramics in Medicine; 2009. pp. 249–52.
40. Varela LM, García M, Mosquera V. Exact mean-field theory of ionic solutions: non-Debye screening. Phys Rep. 2003;382:1–111.
41. Prado Da Silva MH, Lima JHC, Soares GA, Elias CN, de Andrade MC, Best SM, et al. Transformation of monetite to hydroxyapatite in bioactive coatings on titanium. Surf Coat Technol. 2001;137:270–6.
42. Ma M-G, Zhu Y-J, Chang J. Monetite formed in mixed solvents of water and ethylene glycol and its transformation to hydroxyapatite. J Phys Chem B. 2006;110:14226–30.
43. Zavgorodniy AV, Rohanizadeh R, Bulcock S, Swain MV. Ultrastructural observations and growth of occluding crystals in carious dentine. Acta Biomater. 2008;4:1427–39.
44. Gibson IR, Best SM, Bonfield W. Chemical characterization of silicon-substituted hydroxyapatite. J Biomed Mater Res. 1999;44:422–8.
45. Barralet J, Best S, Bonfield W. Carbonate substitution in precipitated hydroxyapatite: an investigation into the effects of reaction temperature and bicarbonate ion concentration. J Biomed Mater Res. 1998;41:79–86.
46. Benjamin P, Weaver C. Measurement of adhesion of thin films. Proc R Soc A. 1960;254:163–76.
47. Bull SJ, Berasetegui EG. An overview of the potential of quantitative coating adhesion measurement by scratch testing. Tribol Int. 2006;39:99–114.
48. Weaver C. Adhesion of thin films. J Vac Sci Technol. 1975;12:18–25.
49. Cui X, Kim H-M, Kawashita M, Wang L, Xiong T, Kokubo T, et al. Preparation of bioactive titania films on titanium metal via anodic oxidation. Dent Mater. 2009;25:80–6.
50. Kokubo T, Miyaji F, Kim H-M, Nakamura T. Spontaneous formation of bonelike apatite layer on chemically treated titanium metals. J Am Ceram Soc. 1996;79:1127–9.